Somatosensory high frequency oscillations across the human central nervous system

Emma Bailey[1*+], Birgit Nierula[1*], Tilman Stephani[2], Vadim Nikulin[2~], Falk Eippert[1~+]

[1] Max Planck Research Group Pain Perception, Max Planck Institute for Human Cognitive and Brain Sciences, Leipzig, Germany

[2] Research Group Neural Interactions and Dynamics, Department of Neurology, Max Planck Institute for Human Cognitive and Brain Sciences, Leipzig, Germany

[*] These authors contributed equally

[~] These authors contributed equally

[+] Corresponding authors

Address for correspondence:

Emma Bailey & Falk Eippert

Max Planck Research Group Pain Perception

Max Planck Institute for Human Cognitive and Brain Sciences

Stephanstraße 1a, 04103, Leipzig, Germany

Number of pages: 31

Number of figures: 6

Number of supplementary pages: 6

Number of supplementary figures: 6

Abstract

Sensory information processing in the central nervous system (CNS) requires both post-synaptic responses and spiking activity, with human electroencephalography (EEG) research largely focused on the former. However, EEG data also contain high-frequency oscillations (HFOs), which have been linked to cortical spike bursts in animal models, thus providing a non-invasive macroscopic marker of population spiking in humans. Here, we go beyond cortical processing and demonstrate that it is possible to simultaneously record HFOs to somatosensory stimulation across the entire human CNS – from spinal cord over subcortical to cortical processing stages. Using multivariate spatial filtering approaches in two independent datasets, we identify replicable and generalizable HFOs across the CNS and obtain a detailed characterization of these signals at each processing level. Finally, we provide evidence at the between- and within-individual level that low and high frequency electrophysiological responses represent at least partly independent information across the CNS. Taken together, our approach offers the first evidence that it is possible to detect and characterise HFOs simultaneously across the CNS, providing a unique non-invasive and multi-level window into human neurophysiology in health and disease.

1. Introduction

Methods for non-invasive and time-resolved recordings of brain function are important tools in human neuroscience and generally fall into two classes: those using indirect read-outs of neuronal function via hemodynamic changes (functional magnetic resonance imaging [fMRI] and functional near infrared spectroscopy [fNIRS]) and those that record direct manifestations of neuronal processes from outside the skull (electroencephalography [EEG] and magnetoencephalography [MEG]). Despite their excellent temporal resolution, the latter largely focus on neuronal signals that have a frequency below ~100Hz – thought to reflect mostly postsynaptic potentials (Baillet, 2017; Biasiucci et al., 2019) – although much faster neuronal signals are ubiquitous throughout the brain.

For example, in the somatosensory domain, small – but very high frequency – notches were seen to overlie low-frequency somatosensory evoked potentials (LF-SEPs) in wide-band EEG recordings after peripheral nerve stimulation (Abbruzzese et al., 1978; Cracco and Cracco, 1976). With improvements in digital filtering approaches, these signals could be isolated from the wideband response, allowing for the study of such high frequency oscillations (HFOs) in their own right in human EEG (Eisen et al., 1984; Yamada et al., 1988) and MEG recordings (Curio et al., 1994; Hashimoto et al., 1996). Importantly, subsequent EEG and MEG recordings in animal models linked HFOs at ~600Hz to spiking activity in somatosensory cortex (Baker et al., 2003; Ikeda et al., 2002; Telenczuk et al., 2011), which is of high interest considering that spikes play a critical role in information transfer between neurons (e.g. for coding sensory and motor parameters). Since recording cortical spike activity in humans is possible only invasively in the context of neurosurgical procedures, HFO recordings via EEG or MEG could offer a unique non-invasive window on cortical population spikes, also complementing the concurrently acquired low-frequency signals of post-synaptic origin.

While the precise cellular substrates that lead to the generation of HFOs are still debated (Coppola, 2004; Gobbelé et al., 2007; Hu et al., 2023; Inoue et al., 2004, 2001; Restuccia et al., 2003), several different experimental approaches have shown somatosensory HFOs to be at least partly independent of their low-frequency counterparts, with differing effects of stimulus repetition (Restuccia et al., 2011), movement (Inoue et al., 2002; Tanosaki, 2002), arousal (Gobbelé et al., 2000), sleep (Hashimoto et al., 1996; Yamada et al., 1988) and anaesthesia (Klostermann et al., 2000). Furthermore, high-frequency neural signals are not limited to the artificial situation of electrical somatosensory nerve stimulation, but are also observed in response to tactile (Baker et al., 2003; Barth, 2003) and visual input (Bishop and Clare, 1953; Funke and Kerscher, 2000) as well as motor cortex stimulation (Beck et al., 2023; Lazzaro et al., 1998).

Considering the existence of HFOs across multiple behavioural domains, one might thus speculate whether they are a neural processing mode that is evident across the entire central nervous system (CNS). Non-invasive support for this comes from dipole source analysis revealing generators in the brainstem, thalamus and cortex (Gobbelé et al., 2007; Halboni et al., 2000), nasopharyngeal recordings showing responses from

the dorsal column pathway at the brainstem level (Restuccia et al., 2004), and surface recordings demonstrating cervical spinal cord responses (Chander et al., 2022); invasive recordings provide further support for this idea (e.g. Berić et al., 1986; Hanajima et al., 2004; Insola et al., 2010, 2008; Jeanmonod et al., 1991; Urasaki et al., 2006).

To the best of our knowledge though, there is a complete lack of systemic approaches that would allow for concurrently recording and characterizing HFOs across the entire CNS. One reason for this is the difficulty in recording them, since HFOs have an amplitude estimated to be over 10 times smaller than typical LF-SEPs (Nakano and Hashimoto, 1999). To overcome this issue, specialised low-noise recording setups have been developed for EEG and MEG (Waterstraat et al., 2021, 2016), but these are currently limited to cortical recordings. Comprehensive recordings across the brain and spinal cord, however, may be crucial for uncovering systematic changes in the spectral and temporal aspects of information propagation throughout the entire CNS.

Here, we therefore used advances in the acquisition (Nierula et al., 2024) and analysis (Bailey et al., 2024; Waterstraat et al., 2015) of non-invasive multi-channel electrophysiological data to probe whether somatosensory HFOs could indeed be concurrently recorded across spinal, subcortical and cortical processing stages. To test the robustness of our experimental approach, this was carried out in two independent studies allowing for direct replication. All recordings were furthermore performed for both upper and lower limb stimulation, as this permitted us to assess the generalizability of our approach. Considering the link between HFOs and neuronal spiking established in cortex (Baker et al., 2003; Ikeda et al., 2002; Telenczuk et al., 2011), such an approach would provide a novel window into neuronal signalling across the entire CNS, potentially offering insights into both fast (spiking) and slow (postsynaptic) neuronal processes.

2. Results

To investigate somatosensory HFOs across the entire CNS, we utilized two independent datasets (Dataset 1: N=36; Dataset 2: N=24) of multichannel surface recordings across the spinal cord and brain in response to electrical peripheral nerve stimulation. We leveraged the multivariate nature of these data to improve the sensitivity of these whole-CNS recordings by using a spatial filtering approach based on canonical correlation analysis (CCA).

2.1. Single participant analyses

Considering that HFOs have not yet been recorded simultaneously across the CNS, we first assessed the ability of our non-invasive approach to detect HFO bursts at the level of single participants. Representative individual time courses (Dataset 1: Figure 1; Dataset 2: Figure S1) demonstrated that there is a distinct HFO burst at each level of the CNS (spinal, subcortical and cortical) with a latency similar to the LF-SEP peak, suggesting that our data quality was sufficient for non-invasively investigating HFOs across the CNS.

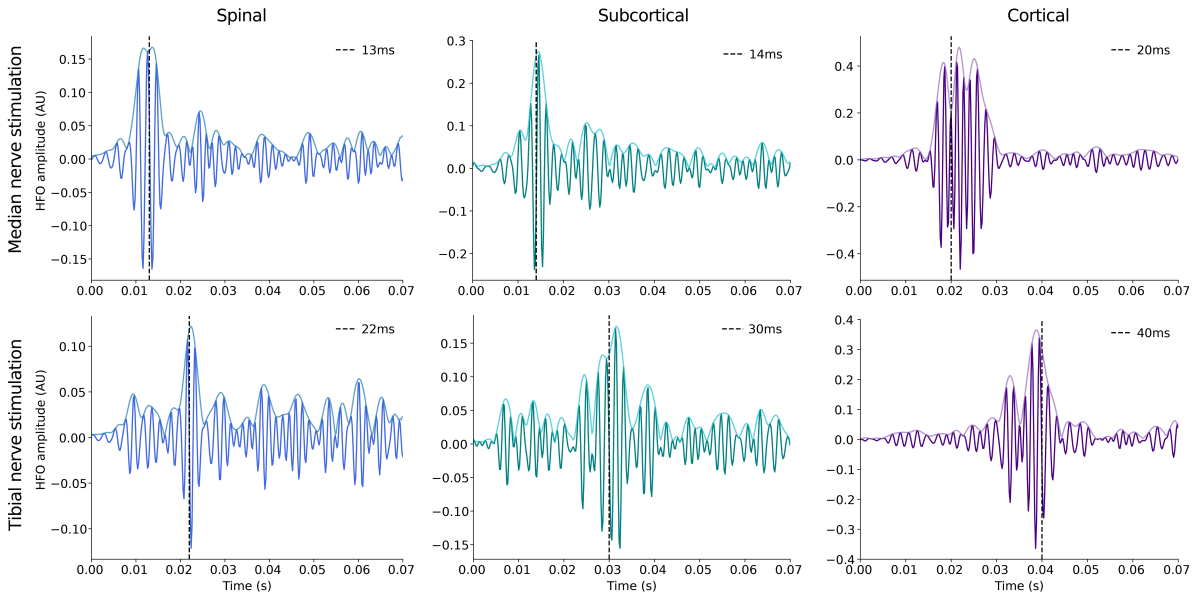

Figure 1. Individual HFO bursts across the CNS. *Single participant HFO time courses after CCA (thick lines) and their amplitude envelopes (thin lines) in response to median nerve stimulation (participant 3: top) and tibial nerve stimulation (participant 31: bottom) across spinal (left), subcortical (middle) and cortical (right) recordings. For each participant, condition and CNS level, the optimal CCA spatial filter was applied to the sensor-space data and plotted in the time-domain as shown here. For each panel, the canonical latency of the LF-SEP is displayed as a dashed vertical line. All data from Dataset 1; a corresponding depiction of data from Dataset 2 can be found in Figure S1.*

This observation was quantitatively supported by the overall proportion of participants in which we were able to identify a CCA component at each CNS level across both datasets (Table 1a): for median nerve stimulation, we were able to identify CCA components at every CNS level in more than 90% of participants and for tibial nerve stimulation a similar proportion emerged at cortical and subcortical levels, though with

lower proportions at the spinal level (52% on average). The advantage offered by our spatial filtering approach is clearly evident when comparing these numbers to those resulting from aiming to detect the HFO burst in sensor space (i.e. prior to the application of the optimal spatial filter; Table 1b): this is almost impossible for tibial nerve stimulation (best-case scenario (Dataset 1, cortex): 19% of participants) and suboptimal even for median nerve stimulation (best-case scenario (Dataset 1, cortex): 75% of participants), with the worst performance at the spinal level. Together, these data demonstrate that spinal, subcortical and cortical HFOs are a robust phenomenon, detectable non-invasively in a large majority of healthy participants when adequate analysis techniques are employed.

Table 1. Proportion of participants with detectable HFOs before and after CCA. *Proportion of participants in which selection criteria were satisfied a) after CCA (i.e. for at least one CCA component) or b) before CCA (i.e. within the channel of interest in sensor space prior to the application of the CCA spatial filters). The rows depict the CNS level and the columns the different datasets. Note that selection was automated and thus not influenced by possible experimenter bias.*

a)	After CCA			
	Median Nerve Stimulation		Tibial Nerve Stimulation	
	Dataset 1	Dataset 2	Dataset 1	Dataset 2
Spinal	35/36	24/24	21/36	11/24
Subcortical	34/36	24/24	35/36	24/24
Cortical	36/36	24/24	36/36	24/24
b)	**Before CCA**			
	Median Nerve Stimulation		Tibial Nerve Stimulation	
	Dataset 1	Dataset 2	Dataset 1	Dataset 2
Spinal	19/36	12/24	0/36	0/24
Subcortical	23/36	15/24	2/36	1/24
Cortical	27/36	14/24	7/36	3/24

2.2. Group level analyses

2.2.1. Time courses and topographies

After establishing the feasibility of concurrent non-invasive HFO detection at spinal, subcortical and cortical levels, we next aimed for a spatiotemporal HFO characterization across the CNS. First, we assessed group-level responses in the time domain, for which it was necessary to average the HFO amplitude envelopes across participants (as slight differences in HFO burst frequency and latency across participants could lead to signal cancellation when averaging HFO time courses). Both for median and for tibial nerve stimulation (Figure 2), we observed clear group-level HFO envelope time courses, though the data in response to tibial nerve stimulation exhibited more noise at all CNS levels. The group-level time courses showed peaks at latencies that are in accordance with the CNS level, with peak latencies for median nerve stimulation at 10.6ms (spinal), 15.2ms (subcortical) and 17.8ms (cortical), and peak latencies for tibial nerve stimulation at 22.4ms (spinal), 31.0ms (subcortical) and 40.4ms (cortical). These results were furthermore replicated in Dataset 2 (Figure S2

and Supplementary Results), with only minimal differences in the observed time courses and peak latencies. There are two further points of note with respect to spinal and subcortical responses. For spinal data, it is interesting to note that although the spinal HFO peak occurs before the canonical 13ms low frequency response to median nerve stimulation, the envelope time-course is clearly above noise level until after this timepoint (though envelope data need to be interpreted carefully due to their non-negative nature). For subcortical data, it is important to point out that the observed peak – with a latency between that of spinal and cortical responses – is not a result that is due to the selected CCA training window (i.e. possible overfitting), but can also be observed to a lesser degree in sensor-space data (Figure S3).

The group-level spatial topographies (Figure 2) aligned with the expected spatial pattern based on the stimulated nerve and central nervous system level, i.e. they were highly similar to what has been observed in low-frequency data. Again, topographies were very similar in the independently acquired Dataset 2 (Figure S2; though note that the subcortical topography to tibial nerve stimulation is rather noisy). Of note, spinal topographies exhibited an additional feature that is not observed in low-frequency data (but replicable across datasets): the cervical response to median nerve stimulation showed an additional lateralized response peak that is ipsilateral to the side of stimulation and could point towards a brachial plexus contribution.

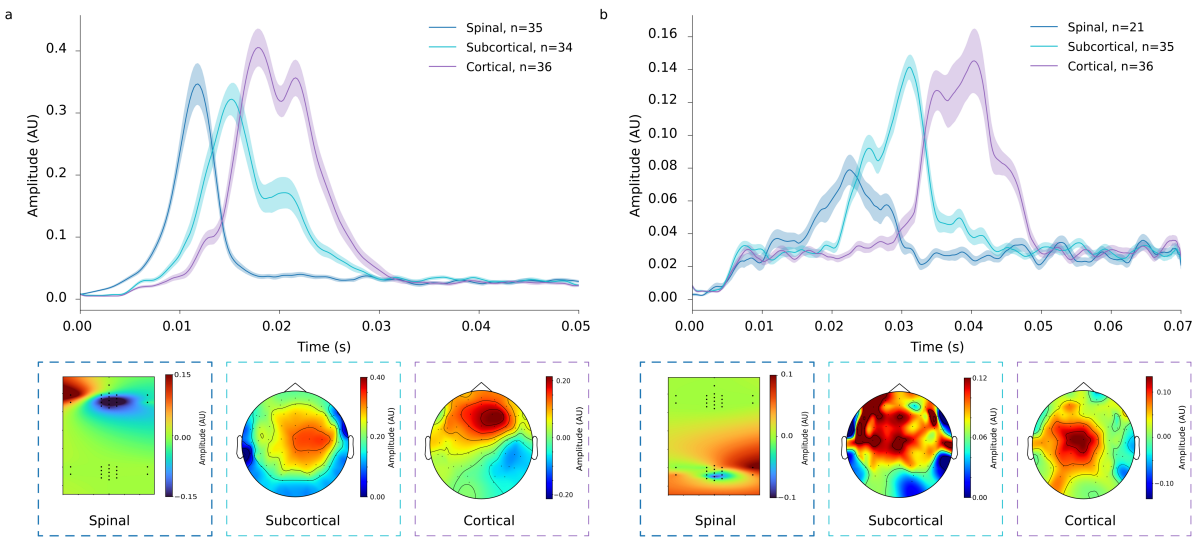

Figure 2. Group-level HFO time courses and topographies across the CNS. *Depicted are group-averaged HFO amplitude envelopes and the associated spatial activation patterns for spinal (black dots representing channel locations), subcortical and cortical responses to a) median nerve stimulation and b) tibial nerve stimulation after the application of CCA. The error bands reflect the SEM across participants and the number of eligible participants entering each average is given in the legend. Please also note that different scales are applied to each plot and that for visualization purposes individual spinal traces were temporally aligned based on the spinal low-frequency peak latency (this was not carried out for peak latency estimation reported above). All data from Dataset 1; a corresponding depiction of data from Dataset 2 can be found in Figure S2.*

Finally, to determine whether CCA extracted genuine stimulus-evoked HFOs, we performed validation analyses involving surrogate (i.e. resting-state) data. We observed that detection of HFOs was consistently more reliable in the stimulation-based compared to the resting-state data (where no stimulation-evoked HFOs should exist): out of the 12 performed analyses (2 datasets x 2 stimulation conditions x 3 CNS levels), 10 analyses showed significantly stronger effects in the stimulation-based data (Table S1); only subcortical and spinal HFOs after tibial nerve stimulation in Dataset 2 failed to pass the significance threshold, possibly also due to power issues caused by the lower participant numbers (N = 11 for spinal level).

2.2.2. Time-frequency representation

Next, we turned to a group-level spectral characterization of HFOs, which is established at the cortical level, but so far elusive across the CNS. Time-frequency representations (TFRs) were obtained for the evoked response to both median and tibial nerve stimulation at each level of the CNS (Figure 3; see Figure S4 for qualitatively similar results in Dataset 2) after applying the optimal spatial filter. The group-level TFRs for both median and tibial nerve stimulation showed areas of increased power relative to baseline in the frequency band of interest (400-800Hz), and at time points relevant to spinal, subcortical and cortical responses, as expected. Importantly, although broadband data are represented (i.e. no spectral filtering has taken place), the high-frequency peaks are clearly distinct from low-frequency activity, with the exception of spinal responses to tibial nerve stimulation where LF and HF bleed into another in Dataset 1 (Figure 3), though not in Dataset 2 (Figure S4). One noteworthy feature in the case of median nerve stimulation is the fact that the frequency of the HFOs appears to increase as one ascends the processing hierarchy from spinal over subcortical to cortical responses, which we next aimed to assess quantitatively.

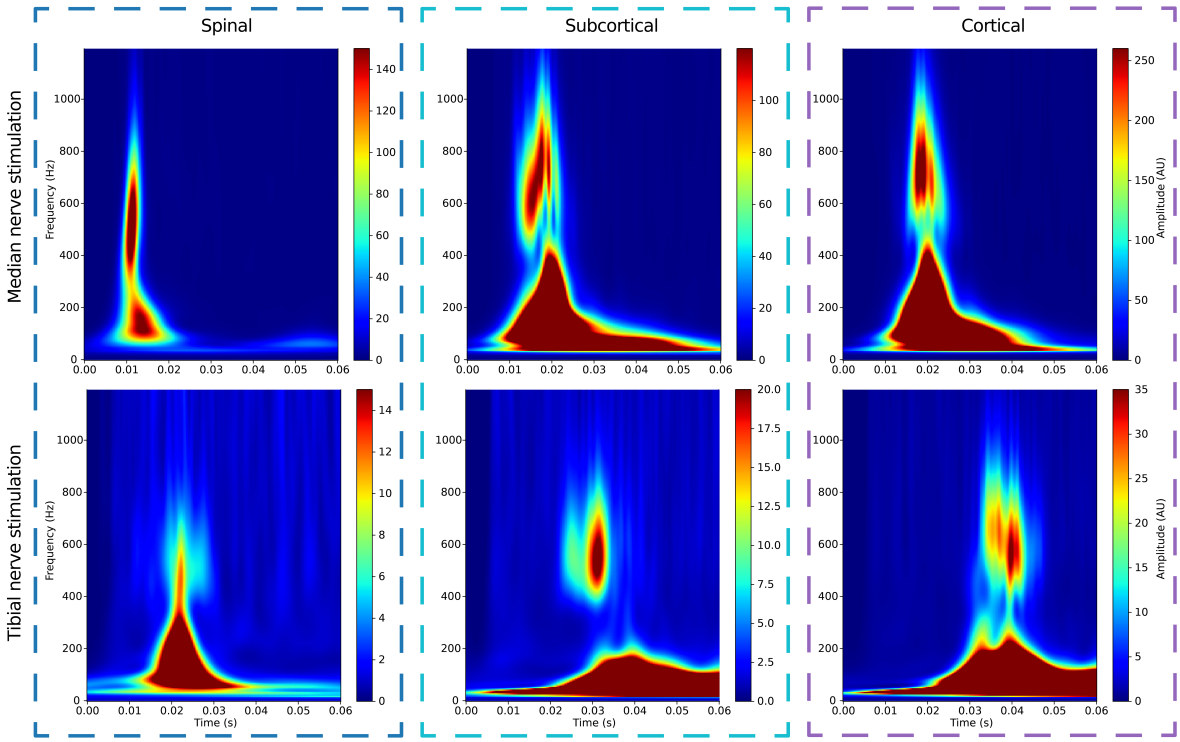

Figure 3. Evoked power across the CNS. *Group-average time-frequency representations of the evoked response to median nerve (top) and tibial nerve (bottom) stimulation, including spinal (left), subcortical (middle) and cortical (right) responses. Please note the different scales applied to each time-frequency plot. All data from Dataset 1; a corresponding depiction of data from Dataset 2 can be found in Figure S4.*

2.2.3. Burst frequency

We therefore calculated the HFO burst frequency for each participant and CNS level, with group-level results presented in Table 2. Descriptively, there appeared to be an increase in HFO burst frequency as the central nervous system is ascended towards the cortical level – this pattern held across both data-sets and both stimulated nerves with the exception of spinal responses to tibial nerve stimulation (where variability across participants is much stronger than in all other cases, see Table 2). Testing this more formally, a repeated measures ANOVA revealed significant differences between the mean burst frequency at different CNS levels in response to median nerve stimulation in both datasets. Follow-up post-hoc paired t-tests revealed that for participants that have an optimal CCA component identified at all levels of the CNS (N=33 in Dataset 1, n=24 in Dataset 2), the spinal burst frequency is significantly lower than the burst frequency at the subcortical level (t=-7.54 for Dataset 1 and t= -6.49 for Dataset 2, both $p<0.05$), and the burst frequency at the subcortical level is significantly lower than the cortical burst frequency (t=-8.70 for Dataset 1 and t=-8.23 for Dataset 2, both $p<0.05$). In response to tibial nerve stimulation, a similar repeated-measures ANOVA failed to reach significance (p=0.055 for Dataset 1 and p=0.09 for Dataset 2), possibly influenced by a lack of power due to the lower number of participants having an optimal CCA component at each level.

Table 2: Group-average burst frequency in Hertz across the central nervous system, expressed as mean ± SEM across participants.

	Median Nerve Stimulation		Tibial Nerve Stimulation	
	Dataset 1	Dataset 2	Dataset 1	Dataset 2
Spinal	528.3 ± 4.7	524.5 ± 5.3	562.7 ± 9.2	580.2 ± 10.3
Subcortical	590.8 ± 7.1	576.8 ± 7.6	552.6 ± 6.8	557.1 ± 7.4
Cortical	652.3 ± 6.8	646.4 ± 6.1	579.6 ± 7.0	580.2 ± 7.9

2.2.4. Wavelet peak count

Since the number (and pattern) of peaks within a cortical HFO wavelet has been related to the number (and pattern) of peaks in single-unit post stimulus time histograms of cortical neurons (Baker et al., 2003; Telenczuk et al., 2011), we next investigated whether the number of peaks within an HFO wavelet would differ across the CNS levels (Figure 4). As an example, for median nerve stimulation we observed a group-average of 4-8 peaks cortically (dependent on the threshold employed for peak detection), while only 2-6 peaks were evident at the spinal level. In general, visual inspection of median nerve stimulation results showed an increase in the number of peaks from spinal over subcortical to cortical levels, while there was no clear trend for responses to tibial nerve stimulation. Importantly, these results held across the various thresholds (for peak definition) we examined, pointing to a robust effect that is not dependent on peak-detection criteria.

When assessing this formally via non-parametric Friedman tests, for both median and tibial nerve stimulation there was a significant effect of CNS-level on peak number at all threshold levels. Follow-up post-hoc Wilcoxon tests further revealed significant differences between spinal-subcortical, and subcortical-cortical wavelet peak counts at each threshold level for median nerve stimulation (all $p<0.05$ after Bonferroni correction), but no significant effects for tibial nerve stimulation. A similar pattern of results was found for Dataset 2 (Figure S5 and Supplementary Results).

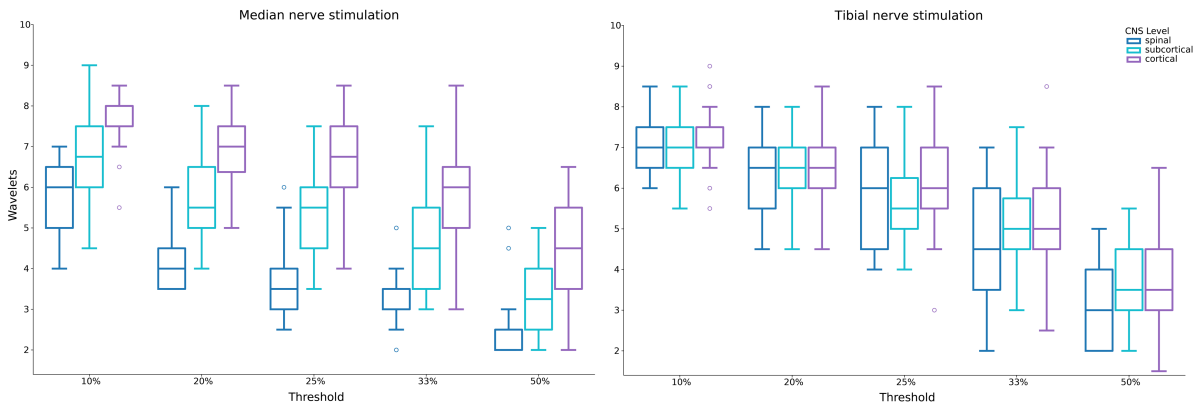

Figure 4. Wavelet peak count across the CNS. *Depicted are the group-average number of wavelet peak bursts at each level of the CNS, dependent on different thresholds used for peak-counting (i.e. relation of peak/trough size to maximum peak/trough, respectively). All data from Dataset 1; a corresponding depiction of data from Dataset 2 can be found in Figure S5.*

2.2.5. Sensory nerve stimulation

Having characterized HFOs across the CNS, we next asked whether our approach would also allow for detecting them in a more challenging scenario with respect to the signal-to-noise ratio (SNR) of HFOs: for this, we used the sensory nerve stimulation conditions of Dataset 2, where a much lower number of nerve fibres is stimulated compared to mixed-nerve stimulation. Our automated component selection procedure revealed that for sensory nerve stimulation of the fingers and toes, there were sufficient participants for statistical analysis only in the case of cortical (18/24) and subcortical responses (7/24) to finger stimulation; neither spinal responses to finger stimulation (2/24) nor any response to toe stimulation (0/24 for all three levels) had enough participants with automatically detected HFOs to perform this analysis.

While there was large inter-individual variability in the strength of the sensory-nerve HFOs (Figure 5), cluster-based permutation testing revealed that it is possible to robustly detect group-level cortical responses after single (finger1, finger2) and double digit (finger12) stimulation, as well as subcortical responses after double digit stimulation. For cortical responses, a significant cluster was identified for finger1 stimulation from 21ms to 33ms (p=0.006), for finger2 stimulation from 18ms to 31ms (p=0.0015) and for finger12 stimulation from 15ms to 33ms (p=0.0005). For subcortical responses, a significant cluster was identified for finger12 stimulation from 15ms to 25ms (p=0.016), while strong but non-significant clusters are identified for finger1 (p=0.063) and finger2 (p=0.086) conditions from 15-19ms and 15-18ms, respectively. Thus, while sensory-nerve HFOs are more difficult to detect, they can still be observed with our approach, which is able to reveal meaningful aspects (e.g. earlier clusters for subcortical than cortical sensory nerve responses).

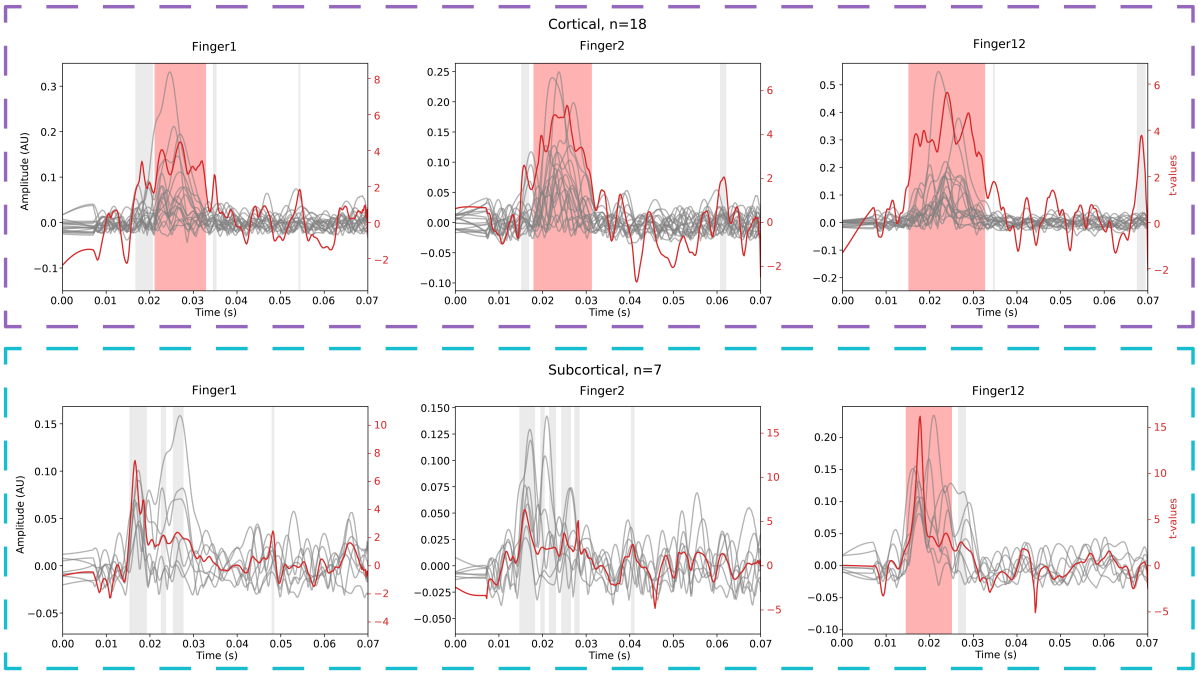

Figure 5. Sensory nerve HFOs. *Gray lines depict participants' individual cortical (top) and subcortical (bottom) amplitude envelopes after single (finger1, finger2) or double (finger12) digit stimulation. The red line depicts the temporally resolved t-values from the cluster-based*

permutation tests (scale on right side of plot), with the shaded areas indicating non-significant (gray) and significant (red) clusters at $p < 0.05$. Please note the different y-axis scaling used in each panel.

2.2.6. Relationship between low-frequency and high-frequency responses

In a final set of analyses, we aimed to probe in two complementary ways – assessing between-participant and within-participant variation – whether low-frequency and high-frequency responses contain redundant information or function as rather independent processing channels.

2.2.6.1. Correlation between average LF-SEP and HFO peak amplitude

First, we investigated whether there would be a significant correlation between average LF-SEP and HFO peak amplitudes across participants, which would speak for these signals containing redundant information. In Dataset 1, significant LF-HF correlations were observed for median-nerve stimulation evoked spinal ($r_{N13} = 0.66$, $p_{N13} < 0.001$) and cortical responses ($r_{N20} = 0.38$, $p_{N20} < 0.05$), but not for tibial-nerve stimulation evoked responses ($r_{N22} = 0.30$, $p_{N22} = 0.19$; $r_{P40} = 0.19$, $p_{P40} = 0.26$). Importantly, when accounting for possibly confounding effects of SNR (by considering the partial correlation controlling for LF-SEP SNR, HFO SNR or both), only the spinal, tibial condition controlling for HFO and LF-SEP SNR showed a significant result ($r_{partial, N22} = 0.54$, $p<0.05$). Dataset 2 showed qualitatively similar results, though here none of the partial correlations were significant (Supplementary Results).

2.2.6.2. Comparing LF-SEP and HFO time courses when considering the strongest versus the weakest trials

Second, we investigated this question at the level of single-trials by selecting the top and bottom 10% of trials based on HFO SNR for each participant and then assessed differences in the evoked response for both LF-SEP and HFO; in case of redundant information, single-trial LF-SEP and HFO amplitudes should be similarly high or low. Using this approach, it was evident that while there was a large difference between the HFO amplitude envelope produced using the strongest versus the weakest 200 trials, there was no perceptible difference between the LF-SEPs when using the same ranking of trials (Figure 6; note that the HFO difference is to be expected, considering that selection and testing are not independent here; the important finding is the absence of differences in the LF-SEP). This pattern was statistically confirmed via cluster-based permutation tests: for spinal data, there was a significant difference in the amplitude envelopes formed using the strongest or the weakest trials for the HFO data between 7ms and 19ms for median nerve stimulation, and between 14ms and 29ms for tibial nerve stimulation (both $p=0.001$), while there was no significant difference in the relevant low frequency SEP traces (not even non-significant clusters were detected). A similar effect was found for cortical data, (significant cluster between 13ms and 26ms for median nerve stimulation and between 32ms and 49ms for tibial nerve stimulation; both $p=0.001$), while there was again no statistically significant difference in the relevant low frequency SEP traces. A comparable pattern of results was observed in Dataset 2 (Figure S6 and Supplementary Results). Together, these results suggest that LF and HF responses represent at least partly independent information channels.

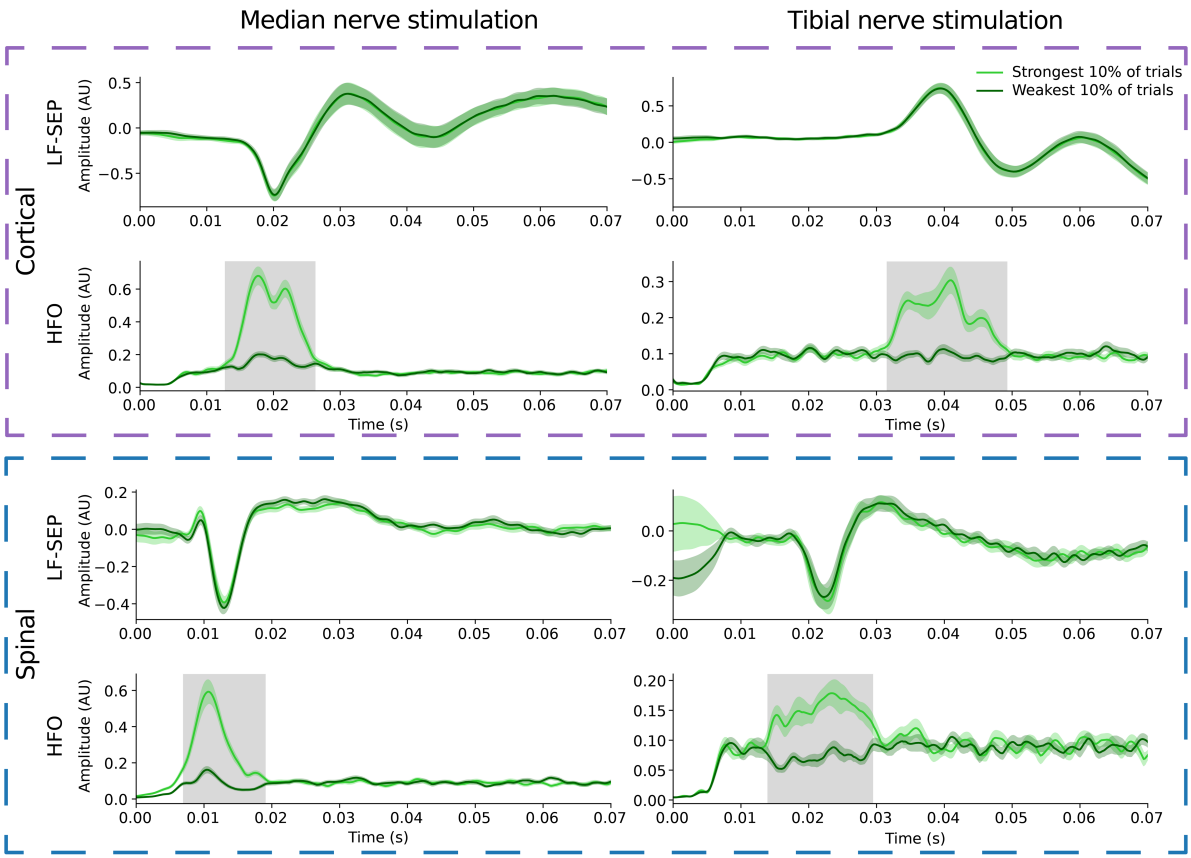

Figure 6. Difference between low-frequency and high-frequency signals. *Depicted are the group-average low-frequency somatosensory evoked potentials (LF-SEP) and group-average high-frequency amplitude envelopes (HFO) when considering either the strongest (light green) or weakest (dark green) 10% of trials (as ranked according to the HFO SNR). The upper two panels show cortical data after median (left; n=36) and tibial (right; n=36) nerve stimulation, whereas the lower two panels show spinal data (median nerve: n=35; tibial nerve: n=20). The grey areas indicate significant clusters at $p < 0.05$ from a cluster-based permutation test. Please note the different y-axis scales employed in each plot. All data from Dataset 1; a corresponding depiction of data from Dataset 2 can be found in Figure S6.*

3. Discussion

In this study, we systematically assessed somatosensory high frequency oscillations (HFOs) to peripheral nerve stimulation across the central nervous system (CNS). While the use of two independent datasets allowed for an internal replication of the obtained results and thus ensured their robustness, the stimulation of both the median nerve (upper limb) and the tibial nerve (lower limb) allowed us to assess the generalizability of our findings. Combining EEG recordings with spinal recordings (via dense multi-channel electrode grids), we observed that it is possible to non-invasively record HFOs in a frequency range of 400-800 Hz – previously linked to population spikes in cortex – from cortical, subcortical and spinal levels, providing a novel and comprehensive window into human neurophysiology.

3.1. Feasibility of non-invasive HFO recordings across the CNS

Although HFOs were discovered almost five decades ago (Abbruzzese et al., 1978; Cracco and Cracco, 1976), it only became apparent in the last two decades that they could provide a novel window into neuronal ensemble activity when their relation to population spikes in cortex was discovered (Baker et al., 2003; Ikeda et al., 2002; Telenczuk et al., 2011). Recent advances in spatial filtering techniques and low-noise data acquisition systems – both developed to address the low SNR of HFOs – have since rekindled interest in these non-invasive macroscopic signals in human neuroscience (Chander et al., 2022; Stephani et al., 2024; Waterstraat et al., 2021, 2015).

Here, we demonstrate that it is possible to obtain somatosensory HFOs across the entire CNS processing hierarchy – from spinal over subcortical to cortical processing sites – using readily available EEG equipment. This represents a critical step forward, as previous invasive (Hanajima et al., 2004; Insola et al., 2010, 2008; Urasaki et al., 2006) and non-invasive HFO studies (Chander et al., 2022; Curio et al., 1997; Gobbelé et al., 1998; Halboni et al., 2000) were only able to provide isolated brain or spinal cord recordings, thus precluding systematic assessments of CNS-level-specific HFO characteristics within a participant. An important aspect of our study was the application of spatial filtering techniques (based on a variant of canonical correlation analysis, CCA; Waterstraat et al., 2015): using such an approach substantially improved the detectability of HFOs across participants (allowing to observe HFOs across all levels in almost every participant after median nerve stimulation) compared to using sensor-level data, suggesting that single-participant HFO studies – e.g. longitudinal dense-sampling approaches – are feasible with the here-developed methods. Three further aspects are important in this regard: i) this CCA-based HFO detection was based on a stringent and automated component selection procedure (eliminating experimenter degrees of freedom), ii) it fared worse in the case of tibial nerve responses in the lumbar spinal cord (where only slightly more than half of all participants showed detectable HFOs), and iii) while CCA might be prone to a certain degree of overfitting (Helmer et al., 2024), we quantitatively addressed this issue via validation analyses involving surrogate resting-state data.

We also probed the current limits of non-invasive entire-CNS HFO recordings by assessing the feasibility of detecting HFOs in response to sensory nerve stimulation, where a >5-fold reduction of activated nerve-fibres is present when stimulating a finger compared to stimulating the median nerve at the wrist (Corniani and Saal, 2020). Here we noticed that i) cortical HFOs were commonly detectable (see also Desmedt and Bourguet, 1985; Ozaki and Hashimoto, 2011) ii) subcortical responses could be assessed when two fingers were stimulated concurrently iii) spinal HFOs could not be assessed at all and iv) detecting HFOs to toe stimulation was not possible at any CNS level. The inability to detect spinal HFOs after finger stimulation contrasts sharply with invasive epidural spinal recordings (Berić et al., 1986) where sensory nerve HFOs are visible and points towards the future need of low-noise recording set-ups in such challenging scenarios. Importantly though, our approach of training CCA on mixed-nerve data (to address the low SNR of sensory-nerve data) could serve as a template when aiming to investigate HFOs to natural tactile stimulation.

3.2. Characteristics of HFOs across CNS levels

Our approach allowed us to characterize HFOs at spinal, subcortical and cortical levels along several features (i.e., latency, topography, frequency, number of wavelet peaks and relation to low-frequency responses). The group-level envelope time-courses demonstrated temporally staggered peaks across spinal, subcortical and cortical levels, occurring at expected time-points based on the canonical LF-SEPs for both upper and lower limb stimulation across both datasets. Interestingly, at the spinal level the peak latency occurred largely before the LF-SEP, which could indicate a predominantly presynaptic nature. The cortical and subcortical HFO topographies were highly similar to their low-frequency counterparts, as observed previously (Curio et al., 1994; Stephani et al., 2020), even though we observed that high-frequency and low-frequency signals carry non-redundant information (see below) and must thus stem from either at least partly independent signal-generating neuronal ensembles (see also Gobbelé et al., 2000; Ogawa et al., 2004) or from distinct processes in different components of pyramidal cells (Stephani et al., 2024). Spinal signals were located centrally in the respective (i.e., cervical or lumbar) electrode patch, though a lateral aspect – possibly indicating brachial plexus contributions – was observed in the case of cervical responses; to our knowledge this constitutes the first spatial description of HFOs along the spinal cord with a dense electrode montage.

Time-frequency assessments in both datasets revealed clear peaks of high-frequency (HF) power that – importantly – were mostly well-separated from low-frequency (LF) power in spinal, subcortical and cortical wideband data. To our knowledge such a clear non-invasive HF-LF distinction has not yet been reported outside of cortex, though invasive spinal recordings (Insola et al., 2008) match our data, also in terms of the spinal peak frequency of around ~500Hz observed here. Leveraging our within-participant design, we could furthermore show a significant increase in HFO frequencies as one ascends the central nervous system from spinal over subcortical to cortical processing stages (apart from the case of lumbar recordings where only few participants were available) – the underlying neurophysiological reason for this hitherto unknown increase within the 400-800Hz frequency band remains to be determined.

By including upper- and lower-limb stimulation conditions, we furthermore observed that at both subcortical and cortical levels, upper-limb HFOs appeared to have higher frequencies across both datasets.

Considering that single peaks in the HFO wavelet have been linked to single peaks in underlying single-unit peristimulus spike histograms (Telenczuk et al., 2011), we next assessed how the number of wavelet peaks evolves across the CNS. In the case of median nerve stimulation, there was a clear and replicable increase across CNS levels in peak counts, that was furthermore independent of the chosen peak threshold criterion (a feature not observed for tibial nerve stimulation). For median nerve stimulation, we observed 2-6 wavelet peaks at the spinal level, which is well in line with invasive recordings (Berić et al., 1986), as are cortical peak counts of 4-8 (Curio et al., 1994; Ozaki et al., 1998); our tibial nerve results are the first such reports to our knowledge. Importantly, our within-participant design allowed us to demonstrate that this increase is of non-random nature as it shows a significant influence of CNS level on peak counts, possibly indicating variations in spiking behavior across these processing stages.

Finally, we demonstrated across both cortex and spinal cord that LF and HF signals are at least partly independent. In a first analysis we observed that the covariation between LF and HF signals across participants was strongly reduced when considering the underlying SNR. In a second analysis that leveraged the increased sensitivity achieved by CCA, we investigated within-participant single-trial dynamics and observed that a highly significant difference in HFO strength was not reflected in LF-SEP strength, where time-courses were virtually identical. Together with earlier data (Chander et al., 2022; Waterstraat et al., 2021) the consistent effects observed here for both between- and within-individual analyses at different CNS levels strengthen the idea that HF and LF signals contain non-redundant information, thus offering a rich window into human neurophysiology that should be exploited when investigating factors that could modulate processing at these levels (e.g. top-down effects (Gijsen et al., 2021) or effects of pathology (Coppola, 2004; Inoue et al., 2004)).

3.3. Neurobiological origin of HFOs in the CNS

The neurobiological origins of cortical HFO bursts have already been well characterized via several invasive and non-invasive studies in animal models (e.g. rats: Jones et al., 2000; pigs: Ikeda et al., 2002; primates: Baker et al., 2003) and humans (e.g. Cimatti et al., 2006; Curio, 2000; Hashimoto, 2000; Urasaki et al., 2006), with a general consensus that the early part of the cortical HFO burst relates to activity in thalamocortical axon terminals, while the latter part relates to intracortical spiking (though the exact identity of cortical neuron types remains to be determined (Hu et al., 2023; Klostermann et al., 2000)). Interestingly, most group-level cortical HFO envelope time-courses observed here had a two-peaked shape, which might map onto these entities. With regards to subcortical responses, only few studies assessed HFOs in the brainstem (e.g. (Halboni et al., 2000; Insola et al., 2010; Restuccia et al., 2004)), though the fast spike-rates of dorsal column nuclei would certainly allow for HFO generation (Calvin and Loeser, 1975). Most research has instead focused on thalamically-generated HFOs, which can either arise from thalamocortical projection

neurons or local activity and can clearly be dissociated from cortical HFOs (Hanajima et al., 2004; Klostermann et al., 2000; Urasaki et al., 2006). In our study, subcortical HFO latencies were compatible with both thalamic and brainstem generators in the case of median nerve stimulation, but the latency of the response favoured a brainstem generator in the tibial nerve condition.

Compared to supraspinal regions, HFO assessment in the spinal cord (carried out here for both the cervical and lumbar cord) is in its infancy: to date, there has been one non-invasive assessment (Chander et al., 2022) and only a few invasive studies in humans (e.g. Berić et al., 1986; Chander et al., 2022; Insola et al., 2008; Jeanmonod et al., 1991; Prestor et al., 1997; Urasaki et al., 2006). As for the cellular substrates that give rise to the here-observed spinal cord HFOs, there are several mutually non-exclusive possibilities: i) activity in afferent terminals upon entry to the dorsal horn (Jeanmonod et al., 1991), ii) complex presynaptic travelling waves in ascending tracts with different conduction velocities (Jeanmonod et al., 1991; Urasaki et al., 2006), and iii) activity of spinal interneurons with spike rates exceeding 500 Hz (Seki et al., 2003). Finally, there could be a contribution from peripheral brachial plexus signals to the early part of an HFO wavelet (Berić et al., 1986; Urasaki et al., 2006), considering the latency and topography of median nerve spinal HFOs observed here. Although the overall peak latency of the observed spinal HFOs might favour a pre-synaptic spiking origin of these signals, we cannot unequivocally establish such a link considering that the envelope time-course also showed heightened HFO activity even after the peak of canonical LF-SEPs in the spinal cord. Here, future HFO studies based on protocols investigating integration (Nierula et al., 2024) or stimulus repetition rate effects (Urasaki et al., 2006) could provide critical insights. Finally, it is worth mentioning that while we were successful in identifying sigma-band HFOs in the spinal cord (i.e. in the range of ~600Hz), distinct higher frequency HFOs in the kappa-band have been identified in cortex non-invasively (Fedele et al., 2012; Waterstraat et al., 2015), and in the spinal cord invasively (Chander et al., 2022; Insola et al., 2008), with invasive data suggesting that the spinal sigma- and kappa-band activity might map onto pre- and postsynaptic spiking, respectively (Insola et al., 2008). In any case, we observed a clear distinction between spinal HFOs and LF-SEPs, strongly suggestive of different information being carried in these two processing channels.

3.4. Limitations and outlook

Several limitations of our approach deserve to be mentioned. First, our investigation of HFOs was restricted by automatically selecting only one CCA component per CNS level. While this allowed for unbiased component selection, it likely does not do justice to the multitude of neuronal processing steps occurring at each level. Future studies could for example subdivide each temporal window to assess HFOs on the rising and falling flank of an LF-SEP peak (Klostermann et al., 1999; Lenoir et al., 2017), which might allow insights into pre- and postsynaptic HFO components at each CNS level by selectively modulating early and late HFOs. Second, our investigation was limited by the low SNR of HFOs, which for example precluded studying responses in the kappa-frequency band (Fedele et al., 2012) or obtaining robust spinal responses to tibial nerve stimulation. Combining our spatial filtering approach with either low-noise-

amplifier technology in EEG (Scheer et al., 2011) or novel SQUID systems in MEG (Waterstraat et al., 2021) could be anticipated to help in such and even more challenging scenarios, such as the sensory nerve stimulation conditions investigated here or recording HFOs to natural tactile stimulation. Third, our multi-channel approach is currently not able to provide spatially resolved insights and could thus benefit from combination with fMRI (Ritter et al., 2008), ideally via techniques with enhanced spatial coverage (Finsterbusch et al., 2013), thus allowing for entire CNS fMRI-HFO recordings. Finally, the insights obtained here solely apply to somatosensory HFOs between 400 and 800 Hz. It is thus unclear to what extent other contexts where fast neuronal signaling in different frequency ranges has been observed – e.g. somatosensory 1kHz HFOs (Fedele et al., 2012) or HFOs in epilepsy below 500Hz (Chen et al., 2021) – would benefit from the methodological approaches developed here.

3.5. Conclusion

In the 100 years since the first electroencephalography (EEG) recording was performed (Mushtaq et al., 2024), EEG research largely focused on signals of cortical origin that typically have frequencies below ~100Hz and are thought to reflect mass post-synaptic activity. Here, using readily available EEG recording equipment, we have critically widened this scope by combining extensions in terms of temporal processing scales (investigating signals up to ~800Hz) and CNS coverage (extending from cortex to spinal cord). Considering the established link between HFOs and population spikes in cortex, the here-observed HFOs could serve as a complementary non-invasive window on neural population activity at various CNS processing stages, both in health and disease.

4. Methods

4.1. Data acquisition

The data used in this study derive from two experiments, with both datasets publicly available (Dataset 1: https://openneuro.org/datasets/ds004388, Dataset 2: https://openneuro.org/datasets/ds004389). Each dataset includes simultaneously recorded electroencephalography (EEG), electrospinography (ESG), electroneurography (ENG), electrocardiography (ECG) and respiratory data. All participants provided written informed consent prior to participation and the study was approved by the Ethics Committee of the Medical Faculty at the University of Leipzig. For the ESG recordings in both datasets, two patches of 17 electrodes each were placed on a participant's neck and lower back: one patch was centred on the cervical spinal cord around an electrode placed over the spinous process of the 6th cervical vertebra and another patch was centred on the lumbar spinal cord around an electrode placed over the spinous process of the 1st lumbar vertebra. The electrodes were arranged along the midline of the vertebral column and extended laterally from there, with the ESG reference electrode being located between the cervical and lumbar electrode patches over the spinous process of the 6th thoracic vertebra. The EEG recordings in Dataset 1 were performed using 64 electrodes with standard positions according to the 10-10 system and referenced to the right mastoid; in Dataset 2 EEG was recorded using 39 electrodes, again referenced to the right mastoid. All data was recorded in an acoustically shielded EEG cabin with a sampling rate of 10kHz and an anti-aliasing filter at 2500Hz with a lower cut-off at 0.16Hz. More details on spinal patch construction as well as electrode placement are available in the original publication (Nierula et al., 2024).

Dataset 1 is comprised of 36 healthy right-handed volunteers (18 female) who received electrical mixed nerve stimulation of the median nerve at the left wrist and of the tibial nerve at the left ankle. Electrical stimulation consisted of a 0.2ms square-wave pulse delivered by constant-current stimulators (DS7A, Digitimer Ltd, Hertfordshire, UK; one stimulator for each nerve) via two bipolar stimulation electrodes. Stimulus intensities were adjusted on an individual level to be just above the motor threshold, but not deemed to be painful. Stimulation occurred with an inter-stimulus interval of 763ms and a uniformly distributed jitter of +/-50ms in steps of 1ms. A total of 2000 stimuli were delivered in alternating blocks of 500 stimuli to either the median or tibial nerve. Further resting state recordings were also performed with eyes open before task-based data acquisition.

Dataset 2 is comprised of 24 healthy right-handed volunteers (12 female), who received electrical mixed nerve stimulation of the median nerve at the left wrist and of the tibial nerve at the left ankle (using the identical equipment as in Dataset 1). In addition to this mixed nerve stimulation, sensory nerve stimulation was also performed by stimulating the fingers or toes using ring electrodes. Finger stimulation occurred in three different ways: to the index finger only (finger1), to the middle finger only (finger2), or to both fingers simultaneously (fingers1&2); the same procedure was used for the toes (toe1, toe2, toes1&2). For mixed nerve stimulation, stimulus intensities were adjusted on an individual level to be just above the motor threshold, while for sensory stimulation conditions the stimulation intensity was set to three times the

detection threshold, as determined by the method of limits. In both cases the stimulation was deemed to be non-painful. Stimulation occurred with an inter-stimulus interval of 257ms and a uniformly distributed jitter of +/-20ms in steps of 1ms. A total of 2000 stimuli were delivered for each mixed nerve and sensory nerve condition. Resting state recordings with eyes open were also performed before task-based data acquisition.

Unless otherwise mentioned, the subsequent preprocessing and analyses are performed on both Dataset 1 and Dataset 2, with the results from Dataset 2 appearing in the supplement.

4.2. ESG and EEG preprocessing

Unless mentioned otherwise, all analyses were performed using Python 3.9 and MNE (https://mne.tools/stable/index.html; version 1.2.0), an open-source toolbox for analysing human neurophysiological data (Gramfort, 2013). In order to remove stimulation artefacts, data were interpolated between -7ms and 7ms relative to stimulus onset for ESG data, and between -1.5ms and 6ms for EEG data using Piecewise Cubic Hermite Interpolating Polynomials (PCHIP). ESG and EEG data were then down sampled to 5kHz, notch filtered around 50Hz with an FIR zero-phase filter and high-pass filtered above 1Hz with a 2nd order Butterworth zero-phase filter. For ESG data, the cardiac artefact was then removed using signal space projection with 6 projectors (Bailey et al., 2024). Bad data segments were annotated if the signal amplitude in the frequency band from 400Hz to 1400Hz was higher than a certain threshold (the mean amplitude across all ESG/EEG channels, plus or minus three times the standard deviation across all ESG/EEG channels); note that a frequency band up to 1400Hz was used as we originally intended to analyse both sigma and kappa band activity (with kappa activity extending to 1200Hz (Fedele et al., 2012)), but were ultimately not able to investigate kappa band activity due to limited SNR in this frequency range. Trials were then marked for exclusion from further analysis based on these annotations. The data was then band pass filtered from 400Hz to 800Hz using a 5th order Butterworth filter to isolate sigma band activity (Fedele et al., 2012).

4.3. Canonical correlation analysis

4.3.1. Training

CCA was performed to optimise the SNR of the HFO activity using the Modular EEG Toolkit (MEET; https://github.com/neurophysics/meet; (Waterstraat et al., 2015)). CCA is used to find the weights w_x and w_y that mutually maximise the correlation

$$\max_{w_x w_y} corr\left(w_x^T X, w_y^T Y\right)$$

where X and Y are both multi-channel signals. We used a variant of CCA also known as canonical correlation average regression (Waterstraat et al., 2015) – in this case, X is a two-dimensional matrix that contains all single-trial epochs from 1 to N for each channel, and Y contains N times the average SEP for each channel. With this

construction, the weight matrix w_x represents the spatial filters that in combination with w_y maximise the correlation between the single trial activity (X) and the average SEP (Y).

The spatial filters w_x were trained using short data segments based on the expected latency and frequency of activity of interest (Table 3), depending on the type of stimulation (median or tibial nerve) and the CNS level under investigation (spinal, subcortical, cortical). For median nerve stimulation, a window of 5ms on either side of the expected peak was used, though in the case of subcortical data, this was reduced to 2.5ms after the expected peak to minimise the effect of cortical activity on the subcortical analysis. For tibial nerve stimulation, due to increased variability of SEP latency across participants, a window of 7.5ms on either side of the expected peak was chosen. Again, in the case of subcortical data, this was reduced to 3.75ms (i.e. 50%) after the expected peak, to remain consistent with the median nerve stimulation analysis.

Table 3: Time windows used for CCA training alongside the expected peak latency at each level of the central nervous system

CNS Level	Median Nerve Stimulation		Tibial Nerve Stimulation	
	Training Window	Expected Peak	Training Window	Expected Peak
Spinal	8ms – 18ms	13ms	14.5ms – 29.5ms	22ms
Subcortical	9ms – 16.5ms	14ms	22.5ms – 33.75ms	30ms
Cortical	15ms – 25ms	20ms	32.5ms – 47.5ms	40ms

For CCA of spinal data, only electrodes from the relevant spinal patch were included (median nerve: cervical patch; tibial nerve: lumbar patch), while for CCA of subcortical and cortical HFOs every EEG electrode was included. Due to the limited SNR for the sensory nerve conditions in Dataset 2, CCA was trained on data from mixed nerve conditions due to their higher SNR and the spatial filters were then applied to the respective mixed and sensory nerve conditions, similar to previous approaches (Nierula et al., 2024). In each case, the resulting spatial filters were applied to the whole length of the epochs from -100ms to 300ms relative to stimulation.

CCA was also performed on the spinal and cortical data prior to the application of spectral filtering from 400-800Hz, in order to obtain the relevant LF-SEPs alongside the HFOs for mixed nerve conditions. This analysis was not done for subcortical responses due to difficulties in identifying the low frequency somatosensory evoked potential for subcortical responses across participants.

4.3.2. Component selection

4.3.2.1. High frequency oscillations

In order to prevent possible experimenter-bias in HFO-component selection, we developed an automated approach, whereby a single CCA component was selected from the top four CCA components (ranked by their canonical correlation coefficient) for each participant and each level of the CNS. To select the optimal component, two criteria were considered:

i) the SNR of the HFO must be above 5,
ii) the peak of the amplitude envelope of the HFO (as computed with a Hilbert transform) must be within the CCA training time window described in Table 3.

The SNR of the HFO was computed as the absolute value of the peak amplitude within the CCA training window, divided by the standard deviation in a noise period from -100ms to -10ms with respect to stimulation. For sensory nerve stimulation (where responses occur with increased latency; (Nierula et al., 2024)), the time window within which the amplitude envelope peak must lie (criterion ii), was the CCA training window shifted rightward by 2ms compared to the mixed nerve condition, and the HFO and its respective envelope was computed across all available conditions combined (i.e. finger1, finger2 and finger12). If there was no component which passed both criteria for a given condition and CNS level, this participant was excluded from further analyses for the given condition and CNS level. If more than one component achieved the specified criteria, the component with the highest SNR was selected.

For each component, the spatial pattern was computed by multiplying the covariance matrix of X by the spatial filters w_x, to take the data's noise structure into account (Haufe et al., 2014). As CCA is insensitive to the polarity of the signal, the optimal component for each participant and condition was manually inspected and marked for inversion if the spatial pattern did not match the expected polarity of a given potential (median: spinal N13, subcortical P14, cortical N20; tibial: spinal N22, subcortical P30, cortical P40).

To demonstrate the benefits of applying spatial filtering, the aforementioned selection criteria were also applied to the data prior to the application of spatial filtering, i.e. selection was performed on data from single channels of interest for median and tibial nerve stimulation respectively (spinal: SC6 and L1, subcortical: CP4 and Cz, cortical: CP4 and Cz after average re-referencing of the data).

4.3.2.2. Low frequency somatosensory evoked potentials

In this case, manual selection of the optimal component was performed by selecting the optimal component among the first four components (as ranked by their canonical correlation coefficient) according to the following criteria in accordance with previous research (Nierula et al., 2024; Stephani et al., 2020):

i) The component time course exhibited a peak at the expected latency
ii) The component spatial pattern exhibited a topography corresponding to the somatotopy of the stimulated nerve

As CCA is insensitive to the polarity of the signal, if the potential at the expected latency of the time course of the chosen component manifested as a positive peak (spinal N13, spinal N22, cortical N20) or a negative peak (cortical P40), the data was inverted.

4.3.3. Validation

We also performed a control analysis to confirm that CCA is identifying genuine stimulus-evoked HFO activity. First, *resting-state* EEG and ESG data were pre-processed in the same manner as described previously for task-evoked data, up to and including the isolation of HFOs by spectrally filtering from 400Hz to 800Hz. In

order to analyse the resting state data in the same manner as the task-evoked data, the resting state data for each participant was concatenated to itself until the length of the resting state data was equal to, or longer than, that of the task-evoked data. Following this, artificial stimulation triggers were added to the resting state data at time points equivalent to their position in the task-evoked data for both the median and tibial nerve condition, before saving these pseudo-task-evoked datasets for each condition. Epochs were then defined spanning from 100ms before to 300ms after the stimulation trigger, with no trials excluded in any participant or condition for either task-evoked or resting state data in this analysis. Following this, during each iteration, 1000 epochs (i.e. 50% of all trials) were subsampled randomly and without replacement from the resting state data and the task-evoked data and submitted to the same CCA procedure as described above for each participant, condition, and CNS level. The first component (as ranked by the canonical correlation coefficient) was selected (without having to satisfy any criteria), and epochs were averaged to form an evoked-response in the case of task-evoked data, and a pseudo evoked-response for resting state data. This process was repeated 1000 times, and after completion, the absolute correlation between each (pseudo) evoked-response and every other (pseudo) evoked-response within the CCA training windows (Table 3) was computed, for resting state and task-evoked data, respectively. The average absolute correlation for each participant, condition and CNS level was then computed by averaging the values in the upper triangle of this 1000x1000 correlation matrix (excluding the main diagonal), to yield a single absolute correlation coefficient in each case. One-sided paired t-tests were then performed to test whether the correlation coefficient was higher in the case of task-evoked data as compared to resting state data within each condition and CNS level.

4.4. Group-level data analyses

4.4.1. Time courses

When presenting group-level time courses, the amplitude envelopes of single participant HFO bursts were averaged, rather than the time courses themselves, as slight differences in the HFO burst frequency and latency across participants could lead to cancellation effects – this is prevented by taking the amplitude envelope. Further, in the case of spinal cord responses, prior to averaging across participants, the HFO bursts were temporally aligned according to the peak latency of each participant's low frequency SEP response for the purpose of visualisation.

4.4.2. Time-frequency representations

Time-frequency representations were obtained for the evoked response for each participant at each CNS level using a Stockwell transform (Stockwell et al., 1996). As CCA was trained using data which was previously band-pass filtered from 400-800Hz, in order to obtain a time-frequency representation across a wider frequency range, the spatial filter of the optimal CCA component was applied to each participants data before band-pass filtering had been performed. This has the added advantage that the data used to generate the time-frequency representations were uncontaminated by potential filter artefacts, such as ringing (Chander et al., 2022). As with the time-courses, for presentation purposes, spinal cord responses were aligned according to the peak latency of each participant's low frequency SEP response.

4.4.3. Burst frequency

The burst frequency was quantified for each participant and CNS level (spinal, subcortical, cortical) for which an optimal CCA component was chosen. First, the optimal spatial filter determined by CCA was applied to the broadband electrophysiology data prior to sigma frequency band isolation, in order to ensure the signal remained uncontaminated by potential filter artefacts. For cortical and subcortical data, channel CP4 was utilised for median nerve stimulation and channel Cz for tibial nerve stimulation. For spinal data, channel SC6 and L1 were used, respectively. These channels represent target locations based on the type of stimulation applied and the processing level under examination. When the spatial filters were applied to the channels of interest, the evoked response was then determined via averaging and subsequently filtered between 400Hz and 800Hz. This filtering was performed to prevent burst frequency detection being affected by the spread of high-power activity from regions outside our interest – this is of particular concern with respect to the low frequency SEP, which has much higher power than the HFOs of interest, and can leak into the higher frequency responses. The time-frequency response was determined using a Stockwell transform and these results were then cropped to form a region of interest, defined in the frequency domain from 400Hz to 800Hz, and in the time domain as the CCA training windows (Table 3). This region was then searched for the maximum power, and the frequency associated with this peak was recorded as the burst frequency.

Repeated-measures ANOVAs were performed to determine whether there were differences between the mean burst frequency at different CNS levels in relation to median and tibial nerve stimulation. If differences were detected, post-hoc two-tailed paired t-tests were also performed (using Bonferroni correction for multiple comparisons).

4.4.4. Wavelet peak count

The number of wavelets contained within an evoked HFO burst was determined for each participant by counting the number of peaks or troughs which were within 7.5ms on either side of the expected SEP latency (Table 3) for median and tibial nerve stimulation. After obtaining the number of peaks and troughs, these values were added together and divided by 2 to obtain the number of bursts. For the majority of analyses, the time window used for median nerve stimulation is shorter than that for tibial nerve stimulation, due to the decreased temporal variability of responses in relation to median nerve stimulation. For this analysis, however, the same time window was used for both median and tibial nerve stimulation analyses, in order to enable comparison between the wavelet counts in relation to both types of stimulation. Peaks/troughs were counted if they were within the designated time window and had an amplitude of at least X% of the maximum HFO peak/trough amplitude within the same time window, with various thresholds examined (X being 10%, 20%, 25%, 33.33% and 50%).

For each condition and threshold, a non-parametric Friedman test was performed to assess whether there were significant differences in the number of wavelets at each level of the CNS. If significant differences were detected, post-hoc two-tailed Wilcoxon signed-rank tests were performed to identify which CNS levels had significant differences (using Bonferroni correction for multiple comparisons).

4.4.5. Sensory nerve stimulation

The ability to detect robust HFOs across participants in response to sensory nerve stimulation at the fingers was tested by means of cluster-based permutation tests for the subcortical and cortical CNS levels. This analysis was not performed for the spinal CNS level after finger stimulation, nor any CNS level after toe stimulation due to the lack of participants with detected HFOs in these cases (all N = 0). For each participant, the amplitude envelope of the HFO time course (created by averaging across all available trials for a given participant) was computed by means of a Hilbert transform. In order to allow for performing cluster-based permutation tests of the signal envelope (which is always above zero), the average amplitude envelopes from each participant were individually baseline corrected by calculating the mean of the amplitude envelope in a noise period (-100ms to -10ms relative to stimulation) and subtracting this value from every time point in the amplitude envelope. Following this, the corrected individual amplitude envelopes were submitted to a one-sided one-sample cluster-based permutation test, separately for each condition (finger1, finger2, finger12) and CNS level (subcortical, cortical).

4.4.6. Relationship between low-frequency and high-frequency responses

Finally, we quantitatively investigated the relationship between the LF-SEP and HFO amplitude in two analyses by asking:

i) across participants, is there a significant correlation between LF-SEP and HFO peak amplitudes (averaging across all trials; resulting in one value for LF-SEP and HFO per participant)

ii) within participants, are the same trials exhibiting maximal/minimal responses for LF-SEP and HFO time courses (considering the top/bottom 10% of trials, as ranked by the single-trial SNR of the HFOs)

For the first analysis, within each participant all trials were averaged and the peaks of the evoked low-frequency (LF-SEP) and high-frequency (HFO) responses were extracted for each condition (within the time windows described in Table 3 for both cortical and spinal data). For LF-SEPs, the polarity of the peak was considered (i.e., a negative peak was searched for with respect to the N20, but a positive peak for the P40) as prior to this analysis each time-course had been inspected after spatial filtering, and if necessary, inverted to match the expected time-course However, for the HFOs the peak amplitude was obtained irrespective of polarity owing the insensitivity of CCA to polarity. This resulted in a single peak amplitude value for each participant, based on their evoked response computed across all trials for a given condition and CNS level, for both the HFO and LF-SEP. The Pearson correlation between the absolute values of these LF-SEP and HFO peak amplitudes was then computed across participants for each condition and CNS level separately. To address the possibly confounding influence of SNR, we i) computed the SNR for the LF-SEPs and HFOs (as the peak amplitude divided by the standard deviation of a pre-stimulus (-100ms to -10ms) noise period and ii) then calculated partial correlations between the LF-SEP and HFO, when controlling for either the LF-SEP SNR, the HFO SNR or both in tandem. This analysis was not performed for subcortical responses due to difficulties in reliably identifying the LF-SEP peak for subcortical responses across participants.

For the second analysis, within each participant all trials were ranked from highest (top) to lowest (bottom) according to the HFO-SNR for the cortical and spinal data after median and tibial nerve stimulation. Separate evoked time-courses were then created for the LF-SEP and HFO amplitude envelope by averaging across either the top or the bottom 10% of trials. The evoked time-course for the bottom 10% of trials was then subtracted from the time-course for the top 10% of trials to form a difference time course for each participant, which were then submitted for statistical assessment at the group level (cluster-based permutation test).

Data and code availability: The underlying data and code are openly available via OpenNeuro (Dataset 1: https://openneuro.org/datasets/ds004388 , Dataset 2: https://openneuro.org/datasets/ds004389) and GitHub (https://github.com/eippertlab/hfo-cns), respectively.

Ethics: All participants gave written informed consent. The study was approved by the Ethics Committee of the Medical Faculty of the University of Leipzig.

Author contributions: Author contributions are listed alphabetically according to CRediT taxonomy (https://credit.niso.org).
Conceptualization: EB, FE, BN, VN, TS
Data curation: BN
Formal analysis: EB
Funding acquisition: FE
Investigation: EB, BN
Methodology: EB, FE, VN
Project administration: EB, FE
Resources: FE, VN
Software: EB
Supervision: FE, VN
Visualization: EB
Writing – original draft: EB, FE
Writing – review & editing: EB, FE, BN, TS, VN

Acknowledgements: We would like to thank all volunteers who participated in this study. Additionally, we want to thank everyone who assisted in data acquisition.

Funding information: FE received funding from the Max Planck Society and the European Research Council (under the European Union's Horizon 2020 research and Innovation Program; grant agreement No 758974).

Competing interest: The authors have no competing interests to declare.

References

Abbruzzese, M., Favale, E., Leandri, M., Ratto, S., 1978. New subcortical components of the cerebral somatosensory evoked potential in man. Acta Neurol. Scand. 58, 325–332. https://doi.org/10.1111/j.1600-0404.1978.tb02896.x

Bailey, E., Nierula, B., Stephani, T., Maess, B., Nikulin, V., Eippert, F., 2024. Evaluating noise correction approaches for non-invasive electrophysiology of the human spinal cord. https://doi.org/10.1101/2024.09.05.611423

Baillet, S., 2017. Magnetoencephalography for brain electrophysiology and imaging. Nat. Neurosci. 20, 327–339. https://doi.org/10.1038/nn.4504

Baker, S.N., Curio, G., Lemon, R.N., 2003. EEG oscillations at 600 Hz are macroscopic markers for cortical spike bursts. J. Physiol. 550, 529–534. https://doi.org/10.1113/jphysiol.2003.045674

Barth, D.S., 2003. Submillisecond Synchronization of Fast Electrical Oscillations in Neocortex. J. Neurosci. 23, 2502–2510. https://doi.org/10.1523/JNEUROSCI.23-06-02502.2003

Beck, M.M., Christiansen, L., Madsen, M.A.J., Jadidi, A.F., Vinding, M.C., Thielscher, A., Bergmann, T.O., Siebner, H.R., Tomasevic, L., 2023. Transcranial magnetic stimulation of primary motor cortex elicits a site-specific immediate transcranial evoked potential. https://doi.org/10.1101/2023.09.05.556160

Berić, A., Dimitrijević, M.R., Prevec, T.S., Sherwood, A.M., 1986. Epidurally recorded cervical somatosensory evoked potential in humans. Electroencephalogr. Clin. Neurophysiol. Potentials Sect. 65, 94–101. https://doi.org/10.1016/0168-5597(86)90041-9

Biasiucci, A., Franceschiello, B., Murray, M.M., 2019. Electroencephalography. Curr. Biol. 29, R80–R85. https://doi.org/10.1016/j.cub.2018.11.052

Bishop, G.H., Clare, M., 1953. SEQUENCE OF EVENTS IN OPTIC CORTEX RESPONSE TO VOLLEYS OF IMPULSES IN THE RADIATION. J. Neurophysiol. 16, 490–498. https://doi.org/10.1152/jn.1953.16.5.490

Calvin, W.H., Loeser, J.D., 1975. Doublet and burst firing patterns within the dorsal column nuclei of cat and man. Exp. Neurol. 48, 406–426. https://doi.org/10.1016/0014-4886(75)90003-5

Chander, B.S., Deliano, M., Azañón, E., Büntjen, L., Stenner, M.-P., 2022. Non-invasive recording of high-frequency signals from the human spinal cord. NeuroImage 253, 119050. https://doi.org/10.1016/j.neuroimage.2022.119050

Chen, Z., Maturana, M.I., Burkitt, A.N., Cook, M.J., Grayden, D.B., 2021. High-Frequency Oscillations in Epilepsy: What Have We Learned and What Needs to be Addressed. Neurology 96, 439–448. https://doi.org/10.1212/wnl.0000000000011465

Cimatti, Z., P Schwartz, D., Bourdain, F., Meunier, S., Bleton, J.-P., Vidailhet, M., Renault, B., Garnero, L., 2006. Time-frequency analysis reveals decreased high-frequency oscillations in writer's cramp. Brain 130, 198–205. https://doi.org/10.1093/brain/awl259

Coppola, G., 2004. Somatosensory evoked high-frequency oscillations reflecting thalamo-cortical activity are decreased in migraine patients between attacks. Brain 128, 98–103. https://doi.org/10.1093/brain/awh334

Corniani, G., Saal, H.P., 2020. Tactile innervation densities across the whole body. J. Neurophysiol. 124, 1229–1240. https://doi.org/10.1152/jn.00313.2020

Cracco, R.Q., Cracco, J.B., 1976. Somatosensory evoked potential in man: Far field potentials. Electroencephalogr. Clin. Neurophysiol. 41, 460–466. https://doi.org/10.1016/0013-4694(76)90057-2

Curio, G., 2000. Linking 600-Hz "Spikelike" EEG/MEG Wavelets ("ς-Bursts") to Cellular Substrates: Concepts and Caveats. J. Clin. Neurophysiol. 17, 377–396. https://doi.org/10.1097/00004691-200007000-00004

Curio, G., Mackert, B.-M., Burghoff, M., Koetitz, R., Abraham-Fuchs, K., Härer, W., 1994. Localization of evoked neuromagnetic 600 Hz activity in the cerebral somatosensory

system. Electroencephalogr. Clin. Neurophysiol. 91, 483–487. https://doi.org/10.1016/0013-4694(94)90169-4
Curio, G., Mackert, B.-M., Burghoff, M., Neumann, J., Nolte, G., Scherg, M., Marx, P., 1997. Somatotopic source arrangement of 600 Hz oscillatory magnetic fields at the human primary somatosensory hand cortex. Neurosci. Lett. 234, 131–134. https://doi.org/10.1016/S0304-3940(97)00690-3
Desmedt, J.E., Bourguet, M., 1985. Color imaging of parietal and frontal somatosensory potential fields evoked by stimulation of median or posterior tibial nerve in man. Electroencephalogr. Clin. Neurophysiol. Potentials Sect. 62, 1–17. https://doi.org/10.1016/0168-5597(85)90030-9
Eisen, A., Roberts, K., Low, M., Hoirch, M., Lawrence, P., 1984. Questions regarding the sequential neural generator theory of the somatosensory evoked potential raised by digital filtering. Electroencephalogr. Clin. Neurophysiol. Potentials Sect. 59, 388–395. https://doi.org/10.1016/0168-5597(84)90040-6
Fedele, T., Scheer, H.J., Waterstraat, G., Telenczuk, B., Burghoff, M., Curio, G., 2012. Towards non-invasive multi-unit spike recordings: Mapping 1kHz EEG signals over human somatosensory cortex. Clin. Neurophysiol. 123, 2370–2376. https://doi.org/10.1016/j.clinph.2012.04.028
Finsterbusch, J., Sprenger, C., Büchel, C., 2013. Combined T2*-weighted measurements of the human brain and cervical spinal cord with a dynamic shim update. NeuroImage 79, 153–161. https://doi.org/10.1016/j.neuroimage.2013.04.021
Funke, K., Kerscher, N., 2000. High-frequency (300–800 Hz) components in cat geniculate (dLGN) early visual responses. J. Physiol.-Paris 94, 411–425. https://doi.org/10.1016/S0928-4257(00)01099-8
Gijsen, S., Grundei, M., Lange, R.T., Ostwald, D., Blankenburg, F., 2021. Neural surprise in somatosensory Bayesian learning. PLOS Comput. Biol. 17, e1008068. https://doi.org/10.1371/journal.pcbi.1008068
Gobbelé, R., Buchner, H., Curio, G., 1998. High-frequency (600 Hz) SEP activities originating in the subcortical and cortical human somatosensory system. Electroencephalogr. Clin. Neurophysiol. Potentials Sect. 108, 182–189. https://doi.org/10.1016/S0168-5597(97)00100-7
Gobbelé, R., Halboni, P., Buchner, H., Waberski, T.D., 2007. Interference of tactile and pain stimuli on thalamocortical signal processing in humans revealed by median nerve SEPs. Clin. Neurophysiol. 118, 2497–2505. https://doi.org/10.1016/j.clinph.2007.08.008
Gobbelé, R., Waberski, T.D., Kuelkens, S., Sturm, W., Curio, G., Buchner, H., 2000. Thalamic and cortical high-frequency (600 Hz) somatosensory-evoked potential (SEP) components are modulated by slight arousal changes in awake subjects. Exp. Brain Res. 133, 506–513. https://doi.org/10.1007/s002210000435
Gramfort, A., 2013. MEG and EEG data analysis with MNE-Python. Front. Neurosci. 7. https://doi.org/10.3389/fnins.2013.00267
Halboni, P., Kaminski, R., Gobbelé, R., Züchner, S., Waberski, T.D., Herrmann, C.S., Töpper, R., Buchner, H., 2000. Sleep stage dependant changes of the high-frequency part of the somatosensory evoked potentials at the thalamus and cortex. Clin. Neurophysiol. 111, 2277–2284. https://doi.org/10.1016/S1388-2457(00)00473-9
Hanajima, R., Chen, R., Ashby, P., Lozano, A.M., Hutchison, W.D., Davis, K.D., Dostrovsky, J.O., 2004. Very Fast Oscillations Evoked by Median Nerve Stimulation in the Human Thalamus and Subthalamic Nucleus. J. Neurophysiol. 92, 3171–3182. https://doi.org/10.1152/jn.00363.2004
Hashimoto, I., 2000. High-Frequency Oscillations of Somatosensory Evoked Potentials and Fields. J. Clin. Neurophysiol. 17.
Hashimoto, I., Mashiko, T., Imada, T., 1996. Somatic evoked high-frequency magnetic oscillations reflect activity of inhibitory interneurons in the human somatosensory cortex. Electroencephalogr. Clin. Neurophysiol. Potentials Sect. 100, 189–203. https://doi.org/10.1016/0168-5597(95)00244-8

Haufe, S., Meinecke, F., Görgen, K., Dähne, S., Haynes, J.-D., Blankertz, B., Bießmann, F., 2014. On the interpretation of weight vectors of linear models in multivariate neuroimaging. NeuroImage 87, 96–110. https://doi.org/10.1016/j.neuroimage.2013.10.067

Helmer, M., Warrington, S., Mohammadi-Nejad, A.-R., Ji, J.L., Howell, A., Rosand, B., Anticevic, A., Sotiropoulos, S.N., Murray, J.D., 2024. On the stability of canonical correlation analysis and partial least squares with application to brain-behavior associations. Commun. Biol. 7, 217. https://doi.org/10.1038/s42003-024-05869-4

Hu, H., Hostetler, R.E., Agmon, A., 2023. Ultrafast (400 Hz) network oscillations induced in mouse barrel cortex by optogenetic activation of thalamocortical axons. eLife 12, e82412. https://doi.org/10.7554/eLife.82412

Ikeda, H., Leyba, L., Bartolo, A., Wang, Y., Okada, Y.C., 2002. Synchronized Spikes of Thalamocortical Axonal Terminals and Cortical Neurons Are Detectable Outside the Pig Brain With MEG. J. Neurophysiol. 87, 626–630. https://doi.org/10.1152/jn.00332.2001

Inoue, K., Harada, T., Kaseda, Y., Mimori, Y., Hashizume, A., Hashimoto, I., Matsumoto, M., 2002. Effects of movement on somatosensory N20m fields and high-frequency oscillations: NeuroReport 13, 1861–1864. https://doi.org/10.1097/00001756-200210280-00006

Inoue, K., Hashimoto, I., Nakamura, S., 2001. High-frequency oscillations in human posterior tibial somatosensory evoked potentials are enhanced in patients with Parkinson's disease and multiple system atrophy. Neurosci. Lett. 297, 89–92. https://doi.org/10.1016/S0304-3940(00)01678-5

Inoue, K., Hashimoto, I., Shirai, T., Kawakami, H., Miyachi, T., Mimori, Y., Matsumoto, M., 2004. Disinhibition of the somatosensory cortex in cervical dystonia—decreased amplitudes of high-frequency oscillations. Clin. Neurophysiol. 115, 1624–1630. https://doi.org/10.1016/j.clinph.2004.02.006

Insola, A., Padua, L., Mazzone, P., Valeriani, M., 2010. Effect of movement on SEPs generated by dorsal column nuclei. Clin. Neurophysiol. 121, 921–929. https://doi.org/10.1016/j.clinph.2010.01.006

Insola, A., Padua, L., Mazzone, P., Valeriani, M., 2008. Unmasking of presynaptic and postsynaptic high-frequency oscillations in epidural cervical somatosensory evoked potentials during voluntary movement. Clin. Neurophysiol. 119, 237–245. https://doi.org/10.1016/j.clinph.2007.09.132

Jeanmonod, D., Sindou, M., Mauguière, F., 1991. The human cervical and lumbo-sacral evoked electrospinogram. Data from intra-operative spinal cord surface recordings. Electroencephalogr. Clin. Neurophysiol. Potentials Sect. 80, 477–489. https://doi.org/10.1016/0168-5597(91)90129-L

Jones, M.S., MacDonald, K.D., Choi, B., Dudek, F.E., Barth, D.S., 2000. Intracellular Correlates of Fast (>200 Hz) Electrical Oscillations in Rat Somatosensory Cortex. J. Neurophysiol. 84, 1505–1518. https://doi.org/10.1152/jn.2000.84.3.1505

Klostermann, F., Funk, T., Vesper, J., Siedenberg, R., Curio, G., 2000. Propofol narcosis dissociates human intrathalamic and cortical high-frequency (> 400 Hz) SEP components: NeuroReport 11, 2607–2610. https://doi.org/10.1097/00001756-200008030-00051

Klostermann, F., Nolte, G., Curio, G., 1999. Multiple generators of 600 Hz wavelets in human SEP unmasked by varying stimulus rates: NeuroReport 10, 1625–1629. https://doi.org/10.1097/00001756-199906030-00001

Lazzaro, V.D., Restuccia, D., Oliviero, A., Profice, P., Ferrara, L., Insola, A., Mazzone, P., Tonali, P., Rothwell, J.C., 1998. Effects of voluntary contraction on descending volleys evoked by transcranial stimulation in conscious humans. J. Physiol. 508, 625–633. https://doi.org/10.1111/j.1469-7793.1998.625bq.x

Lenoir, C., Huang, G., Vandermeeren, Y., Hatem, S.M., Mouraux, A., 2017. Human primary somatosensory cortex is differentially involved in vibrotaction and nociception. J. Neurophysiol. 118, 317–330. https://doi.org/10.1152/jn.00615.2016

Mushtaq, F., Welke, D., Gallagher, A., Pavlov, Y.G., Kouara, L., Bosch-Bayard, J., Van Den Bosch, J.J.F., Arvaneh, M., Bland, A.R., Chaumon, M., Borck, C., He, X., Luck, S.J., Machizawa, M.G., Pernet, C., Puce, A., Segalowitz, S.J., Rogers, C., Awais, M., Babiloni, C., Bailey, N.W., Baillet, S., Bendall, R.C.A., Brady, D., Bringas-Vega, M.L., Busch, N.A., Calzada-Reyes, A., Chatard, A., Clayson, P.E., Cohen, M.X., Cole, J., Constant, M., Corneyllie, A., Coyle, D., Cruse, D., Delis, I., Delorme, A., Fair, D., Falk, T.H., Gamer, M., Ganis, G., Gloy, K., Gregory, S., Hassall, C.D., Hiley, K.E., Ivry, R.B., Jerbi, K., Jenkins, M., Kaiser, J., Keil, A., Knight, R.T., Kochen, S., Kotchoubey, B., Krigolson, O.E., Langer, N., Liesefeld, H.R., Lippé, S., London, R.E., MacNamara, A., Makeig, S., Marinovic, W., Martínez-Montes, E., Marzuki, A.A., Mathew, R.K., Michel, C., Millán, J.D.R., Mon-Williams, M., Morales-Chacón, L., Naar, R., Nilsonne, G., Niso, G., Nyhus, E., Oostenveld, R., Paul, K., Paulus, W., Pfabigan, D.M., Pourtois, G., Rampp, S., Rausch, M., Robbins, K., Rossini, P.M., Ruzzoli, M., Schmidt, B., Senderecka, M., Srinivasan, N., Stegmann, Y., Thompson, P.M., Valdes-Sosa, M., Van Der Molen, M.J.W., Veniero, D., Verona, E., Voytek, B., Yao, D., Evans, A.C., Valdes-Sosa, P., 2024. One hundred years of EEG for brain and behaviour research. Nat. Hum. Behav. 8, 1437–1443. https://doi.org/10.1038/s41562-024-01941-5

Nakano, S., Hashimoto, I., 1999. Comparison of somatosensory evoked high-frequency oscillations after posterior tibial and median nerve stimulation. Clin. Neurophysiol. 110, 1948–1952. https://doi.org/10.1016/S1388-2457(99)00145-5

Nierula, B., Stephani, T., Bailey, E., Kaptan, M., Pohle, L.-M., Horn, U., Mouraux, A., Maess, B., Villringer, A., Curio, G., Nikulin, V.V., Eippert, F., 2024. A multi-channel electrophysiology approach to non-invasively and precisely record human spinal cord activity. https://doi.org/10.1101/2022.12.05.519148

Ogawa, A., Ukai, S., Shinosaki, K., Yamamoto, M., Kawaguchi, S., Ishii, R., Takeda, M., 2004. Slow repetitive transcranial magnetic stimulation increases somatosensory high-frequency oscillations in humans. Neurosci. Lett. 358, 193–196. https://doi.org/10.1016/j.neulet.2004.01.038

Ozaki, I., Hashimoto, I., 2011. Exploring the physiology and function of high-frequency oscillations (HFOs) from the somatosensory cortex. Clin. Neurophysiol. 122, 1908–1923. https://doi.org/10.1016/j.clinph.2011.05.023

Ozaki, I., Suzuki, C., Yaegashi, Y., Baba, M., Muneo Matsunaga, Hashimoto, I., 1998. High frequency oscillations in early cortical somatosensory evoked potentials. Electroencephalogr. Clin. Neurophysiol. Potentials Sect. 108, 536–542. https://doi.org/10.1016/S0168-5597(98)00032-X

Prestor, B., Gnidovec, B., Golob, P., 1997. Long sensory tracts (cuneate fascicle) in cervical somatosensory evoked potential after median nerve stimulation. Electroencephalogr. Clin. Neurophysiol. Potentials Sect. 104, 470–479. https://doi.org/10.1016/S0168-5597(97)00040-3

Restuccia, D., Della Marca, G., Valeriani, M., Rubino, M., Scarano, E., Tonali, P., 2004. Brain-stem components of high-frequency somatosensory evoked potentials are modulated by arousal changes: nasopharyngeal recordings in healthy humans. Clin. Neurophysiol. 115, 1392–1398. https://doi.org/10.1016/j.clinph.2004.01.015

Restuccia, D., Marca, G.D., Valeriani, M., Rubino, M., Paciello, N., Vollono, C., Capuano, A., Tonali, P., 2003. Influence of cholinergic circuitries in generation of high-frequency somatosensory evoked potentials. Clin. Neurophysiol. 114, 1538–1548. https://doi.org/10.1016/S1388-2457(03)00138-X

Restuccia, D., Piero, I.D., Martucci, L., Zanini, S., 2011. High-frequency oscillations after median-nerve stimulation do not undergo habituation: A new insight on their functional meaning? Clin. Neurophysiol. 122, 148–152. https://doi.org/10.1016/j.clinph.2010.06.008

Ritter, P., Freyer, F., Curio, G., Villringer, A., 2008. High-frequency (600 Hz) population spikes in human EEG delineate thalamic and cortical fMRI activation sites. NeuroImage 42, 483–490. https://doi.org/10.1016/j.neuroimage.2008.05.026

Scheer, H.J., Fedele, T., Curio, G., Burghoff, M., 2011. Extension of non-invasive EEG into the kHz range for evoked thalamocortical activity by means of very low noise amplifiers. Physiol. Meas. 32, N73–N79. https://doi.org/10.1088/0967-3334/32/12/n02

Seki, K., Perlmutter, S.I., Fetz, E.E., 2003. Sensory input to primate spinal cord is presynaptically inhibited during voluntary movement. Nat. Neurosci. 6, 1309–1316. https://doi.org/10.1038/nn1154

Stephani, T., Villringer, A., Nikulin, V.V., 2024. Excitability modulations of somatosensory perception do not depend on feedforward neuronal population spikes. https://doi.org/10.1101/2024.07.15.603430

Stephani, T., Waterstraat, G., Haufe, S., Curio, G., Villringer, A., Nikulin, V.V., 2020. Temporal Signatures of Criticality in Human Cortical Excitability as Probed by Early Somatosensory Responses. J. Neurosci. 40, 6572–6583. https://doi.org/10.1523/JNEUROSCI.0241-20.2020

Stockwell, R.G., Mansinha, L., Lowe, R.P., 1996. Localization of the complex spectrum: the S transform. IEEE Trans. Signal Process. 44, 998–1001. https://doi.org/10.1109/78.492555

Tanosaki, M., 2002. Movement interference attenuates somatosensory high-frequency oscillations: contribution of local axon collaterals of 3b pyramidal neurons. Clin. Neurophysiol. 113, 993–1000. https://doi.org/10.1016/S1388-2457(02)00114-1

Telenczuk, B., Baker, S.N., Herz, A.V.M., Curio, G., 2011. High-frequency EEG covaries with spike burst patterns detected in cortical neurons. J. Neurophysiol. 105, 2951–2959. https://doi.org/10.1152/jn.00327.2010

Urasaki, E., Maeda, R., Akamatsu, N., Yokota, A., 2006. Chapter 22 Origins and characteristics of high-frequency (>500 Hz) SEP components directly recorded from the cervical cord, thalamus, and cerebral cortex, in: Supplements to Clinical Neurophysiology. Elsevier, pp. 159–165. https://doi.org/10.1016/S1567-424X(09)70026-1

Waterstraat, G., Fedele, T., Burghoff, M., Scheer, H.-J., Curio, G., 2015. Recording human cortical population spikes non-invasively – An EEG tutorial. J. Neurosci. Methods 250, 74–84. https://doi.org/10.1016/j.jneumeth.2014.08.013

Waterstraat, G., Körber, R., Storm, J.-H., Curio, G., 2021. Noninvasive neuromagnetic single-trial analysis of human neocortical population spikes. Proc. Natl. Acad. Sci. 118, e2017401118. https://doi.org/10.1073/pnas.2017401118

Waterstraat, G., Scheuermann, M., Curio, G., 2016. Non-invasive single-trial detection of variable population spike responses in human somatosensory evoked potentials. Clin. Neurophysiol. 127, 1872–1878. https://doi.org/10.1016/j.clinph.2015.12.005

Yamada, T., Kameyama, S., Fuchigami, Y., Nakazumi, Y., Dickins, Q.S., Kimura, J., 1988. Changes of short latency somatosensory evoked potential in sleep. Electroencephalogr. Clin. Neurophysiol. 70, 126–136. https://doi.org/10.1016/0013-4694(88)90113-7